2024 IEEE/RSJ International Conference on Intelligent Robots and Systems (IROS)
October 14-18, 2024. Abu Dhabi, UAE

Wirelessly Actuated Rotation-free Magnetic Motor

Umur Ulas Harman[1], Ahmed Hafez[1], Cameron Duffield[1], Zihan Zhao[1],
Luke Dixon[1], Daniela Rus[2] and Shuhei Miyashita[1,3]

***Abstract*— This paper addresses the challenge of actuating millimetre-sized motors, which are wirelessly driven by external magnetic fields. Traditional approaches, relying on rotating magnetic fields, often inadvertently cause the entire robot – especially if it is small and lightweight – to rotate, instead of a specified shaft in the motor. To overcome this issue, our study introduces a novel mechanism that leverages symmetrically configured magnetic motors to cancel out the torques, thus preventing unwanted rotation of the robot. This is achieved by utilizing a magnetic field along a single axis to induce rotational movement. The design features two millimetre-sized rotating magnets that interact to achieve a 90° rotation, complemented by an external magnetic field that accomplishes the remaining 270°, thus completing a full rotation. Furthermore, we demonstrate that applying a perpendicularly oriented magnetic field can inversely affect the motor's rotation direction. A proof-of-concept experiment employing this mechanism successfully actuated a gripper in a water tank while it is free-floating, showcasing its potential for enhancing robotic applications at the sub-centimeter scale, where the small net torque of a miniature motor is essential.**

I. Introduction

Small robots designed for internal use in the body benefit from being electronics-free, enhancing their reliability, potential for miniaturization, and biocompatibility [1], [2], [3]. Various alternative methods to electronics-based actuation, such as (1) air pressure, (2) chemical reactions, (3) shape-memory polymers, and (3) magnetic fields, have been employed to move and control these robots without the need for onboard circuits or batteries [4], [5], [6]. Magnetic interactions are especially promising, enabling untethered motion in confined hard-to-reach areas [7], [8], [9], [10]. Complex motions can be achieved by using moving permanent magnets or electromagnets that create a specific magnetic field or field gradient, thus actuating robots equipped with magnetic materials [11], [12], [13], [14]. In medical settings, external magnetic sources, like MRI devices, could provide the necessary magnetic fields, eliminating the need for internal electronics in the robots [15], [16], [17], [18], [19], [20], [21].

Magnetic actuation faces a significant limitation: the strength of the magnetic force decreases quickly as the distance from the field source increases or the robot's magnetic volume decreases [22], [23]. Consequently, to achieve the necessary magnetic forces without reducing the size of the workspace, large and costly electromagnets may be required. Moreover, certain movements, such as rotation around the robot's magnetization axis, cannot be accomplished unless using an advanced magnetic actuation technique [24]. A potential solution involves enhancing the forces and torques from magnetic actuation through a mechanical transmission system equipped with gears [2]. This gearbox, integrating a permanent magnet, rotates under an externally applied rotating magnetic field, enabling it to produce high torques for complex functions like jumping, sampling, and peristaltic movement. However, robots equipped with magnetically-actuated motors and gearboxes [2], [10] often experience a net torque that causes unwanted rotations, potentially compromising functionality [25], [26]. The reactive frictional force must be sufficiently strong to counteract any rotational motion, limiting these robots' usability in environments where controlling surface frictional properties is difficult.

In this study, we developed a novel magnetically-actuated motor that operates in response to a reversible bi-axial

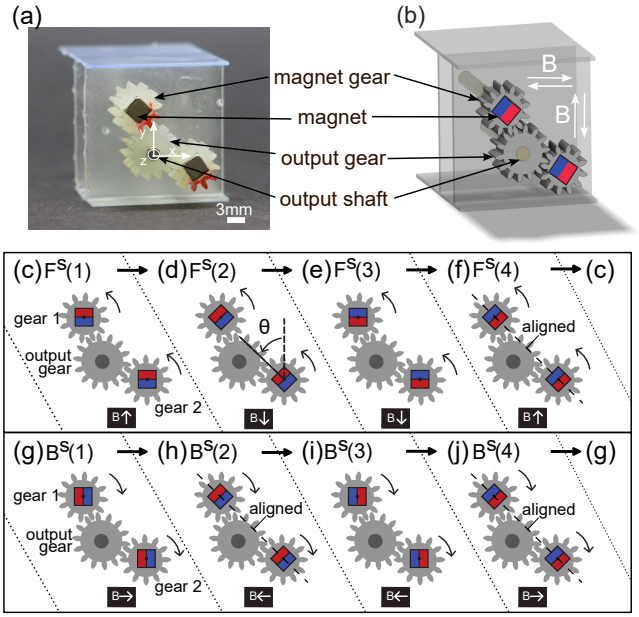

Fig. 1. The proposed magnetic motor. (a) Photo of the motor, (b) CAD design of the motor. Each state (c to j) shows a snapshot during the operation of the motor during counter-clockwise (c to f) and clockwise (g to j) rotation at different magnet orientations θ. The direction of the applied magnetic flux B is shown below each state, consistent with the local coordinate system. For example, $B\uparrow$ indicates that the magnetic field is applied in the positive direction of the y-axis. Note that in the absence of an externally applied magnetic field, the motor can assume either states (d) / (h) or (f) / (j). During forward and backward rotation, states (d), (f), (h) and (j) are achieved momentarily during motor operation while the field remains on, see Fig. 2.

[1]Automatic Control and Systems Engineering Department, University of Sheffield, Sheffield S1 3JD, UK. uuharman1@sheffield.ac.uk
[2]Computer Science and Artificial Intelligence Laboratory, Massachusetts Institute of Technology, Cambridge, MA, USA. [3] Insigneo Institute for *in silico* Medicine. Support for this work has been provided by Turkey's Ministry of National Education and the EPSRC grant EP/X029034/1 and NSF grants 1240383 and 1138967.

magnetic field along two perpendicular directions, rather than a rotating magnetic field. The rotation of the two magnets in each motor depends on the interplay between their mutual interaction and their response to the externally-applied magnetic field. We then developed a rotation-free dual-motor system composed of two motors with four embedded permanent magnets. We arrange the component gears and magnets in a configuration that generates net zero torque. Thus, the dual-motor system and any attached components or robots do not experience undesired rotations, regardless of the frictional properties of the underlying surface. Unlike previously-developed magnetic motors and gears [2], our dual-motor system requires a simple electromagnetic coil setup that generates a bi-axial field along two perpendicular directions for actuation.

We arrange this study as follows. In Section II-A we present the design of a single motor and develop a mathematical model that estimates the resultant torque at different motor orientations. We then use this model to optimize the design of the motor, by studying the effect of the magnet size and spacing between magnets on the output torque (Section II-B). We then adopt the optimized motor design to make the dual-motor system in Section II-C. Finally, we demonstrate the performance of the dual-motor system with a rotation-free mini-gripper in Section IV. Section V summarizes the salient conclusions from this study.

II. The Mechanism and the Model

A. The rotation-free magnetic motor

The developed magnetically-actuated motor (Fig. 1 (a) and (b)) consists of three gears meshed together. The two side gears (called magnet gears) each contain a cubic NdFeB magnet (magnet size: $3 \times 3 \times 3\,\text{mm}^3$) glued in a dedicated compartment at the center (magnet gear module is $0.5\,\text{mm}$, number of teeth is 12). The rotation of the magnet gears cause the output gear at the center of the motor to rotate, thus delivering torque through the output shaft at the center of the gear (output gear module is 0.5 mm, number of teeth is 14, shaft diameter is 1 mm). The gear reduction ratio of the overall motor appearing in (Fig. 1 (a)) is 1:1.17, which can vary by altering the module of the output gear depending on the operational requirements.

In the absence of an externally applied magnetic field, the magnetic moment vector of each magnet (the line joining the two magnetic poles) is oriented at an angle of θ=45°, where θ is the angle between the magnetic moment vector $\vec{m}$ and the external magnetic flux $\vec{B}_{ext}$. The two permanent magnets in the motor rotate in response to an externally applied magnetic field generated from a nearby electromagnetic coil, which can generate a magnetic flux density B_{ext} until $14\,\text{mT}$ in either the x or y direction (following the local coordinate system shown in (Fig. 1 (a)).

The resultant rotation of the magnets in the motor depends on the interplay between the externally applied magnetic field, the intrinsic fields of the magnets and their mutual interactions (Fig. 1 (c) to (f)). First, the two magnets experience a torque τ_{ext} and rotate until their respective magnetic moments coincide with the direction of the external field from the coils (state $F^s(1)$ in Fig. 1 (c)), at that point τ_{ext} drops to zero. We then reverse the direction of the external field. The mutual attraction between the two magnets then causes them to continue their counter-clockwise rotation until their respective magnetic moments align along a common axis (state $F^s(2)$ in Fig. 1 (d)). We call this torque that results from the mutual attraction of the magnets as the internal torque τ_{int}. The newly established external field direction forces the magnets to rotate one more time along the same direction (reaching state $F^s(3)$ in Fig. 1 (e)), and the cycle ends after the field reverses again (state $F^s(4)$ in Fig. 1 (f)). The total torque on the motor, τ_{tot}, at any given time is thus: $\tau_{tot} = \tau_{int} + \tau_{ext}$.

A highlight of the motor developed in this study is its reversibility. The motor can rotate in the opposite (or clockwise) direction simply by applying a magnetic field along the perpendicular direction (Fig. 1 (g) to (j)). Thus, we place another coil perpendicular to the first one and position the motor between the two perpendicular coils. One coil generates a field that causes the motor to rotate clockwise, while the other coil causes the motor to rotate counter-clockwise. We use four coils placed perpendicular to each other in some applications to improve the uniformity of the field and increase the size of the available workspace.

The operation and intermediate states during the clockwise rotation are analogous to the counter-clockwise case. The external torque causes the magnets to align their magnetic moments in the direction of the external magnetic field (state $B^s(1)$ in Fig. 1 (g)), the field reverses, the internal torque aligns the moments of both magnets along a common axis (state $B^s(2)$ in Fig. 1 (h)), the external torque then causes the magnets to align to the new field direction (state $B^s(3)$ in Fig. 1 (i)) and the magnets complete the cycle after we reverse the field again (state $B^s(4)$ in Fig. 1 (j)).

B. Characterization of the magnetically actuated motor

1) The output torque: We now develop a mathematical model that estimates the output torque of a single motor at different magnet orientations θ (rad). Results and insights from this model will help optimize the design of the motor to deliver higher output torques.

Using the magnetic dipole model, we can calculate the internal magnetic torque that magnet i ($i \in [1,2]$) with magnetic moment $\vec{m}_i$ experiences from magnet j ($j \in [1,2]$, $j \neq i$) with magnetic moment $\vec{m}_j$, $\tau_{int,ij}$, which results from the mutual interaction between two magnets [27]:

$$\vec{\tau}_{int,ij} = \frac{\mu_0}{4\pi\|r_{ij}\|^5} \cdot \{3\,\vec{m}_j \times (\vec{m}_i \cdot \vec{r_{ij}})\,\vec{r_{ij}} - r_{ij}^2(\vec{m}_j \times \vec{m}_i)\}, \quad (1)$$

where $\|\vec{m}_i\| = \|\vec{m}_j\| = 0.0258\,\text{Am}^2$ for the magnets used in this study, $\mu_0 = 1.256{\cdot}10^{-6}\,\text{NA}^{-2}$ is the permeability of free space and $\vec{r}_{ij}$ is the vector that joins the centers of the two magnets originating from magnet j, $\vec{r}_{ij} = \|\vec{r}_{ij}\| \cdot [-1, 1, 0]^T$

for the configuration shown in Fig. 1. The magnitude of $\vec{r}_{ij}$ represents the magnet spacing.

The external magnetic torque that magnet i experiences, $\tau_{ext,i}$ and acts to align the magnet towards the direction of the external field is given by:

$$\vec{\tau}_{ext,i} = \vec{m}_i \times \vec{B}_{ext}, \tag{2}$$

where $\vec{B}_{ext}$ represents the magnetic flux density generated by the coils.

Finally, we obtain the total output torque that the motor delivers, $\vec{\tau}_{mot}$, as

$$\vec{\tau}_{mot} = GR \cdot (\vec{\tau}_{ext,i} + \vec{\tau}_{ext,j} + \vec{\tau}_{int,ij}), \tag{3}$$

where GR is the gear reduction ratio of the magnet gear and the output gear ($GR = 1.17$ for our motor).

Fig. 2 shows the internal torque experienced by magnet i from magnet j ($\tau_{int,ij}$), external torque experienced by magnet i ($\tau_{ext,i}$) and the output motor torque (τ_{mot}), over angle θ, derived from Eqs. (1), (2) and (3).In the absence of an applied magnetic field or when $\tau_{ext,i}$=0, τ_{mot} is higher than $\tau_{int,ij}$ because the gear ratio GR>1, Eq. (3).

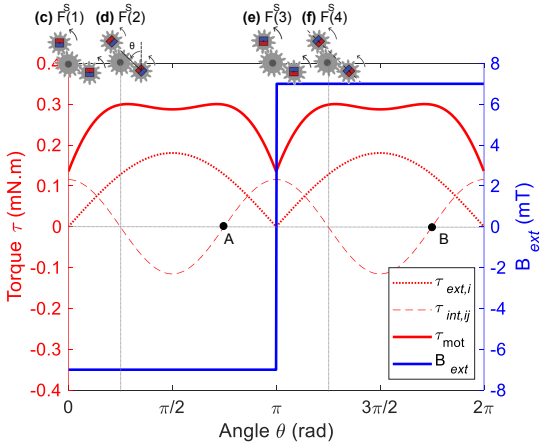

Fig. 2. The theoretically derived internal magnetic torque experienced by magnet i from magnet j ($\tau_{int,ij}$), external magnetic torque that magnet i experiences ($\tau_{ext,i}$, which is the same as m_j experiences), and the output torque of the motor (τ_{mot}) over one revolution of the output shaft.

It shows that the magnets experience the highest external torque when their respective magnetic moments are perpendicular to the external field direction (at $\theta = \pi/2$ and $\theta = 3\pi/2$). The internal torque is zero when the moments of both magnets lie along a common axis, which corresponds to the equilibrium position ($\theta = \pi/4$ and $\theta = 5\pi/4$). Note that, in practice, we do not observe a stable equilibrium configuration with zero internal torque when the magnets are parallel at ($\theta = 3\pi/4$ and $\theta = 7\pi/4$, points A and B in Fig. 2). A steeper curve is expected at points A and B in a more accurate model, but this is not critical to the behavior of the motor and is not the focus of this study.

We now use the model to optimize the design of the motor. Fig. 3 (a) shows the effect of the magnets' size, and hence the strength of its local magnetic field, on the output torque of the motor at constant spacing r=12 mm. Bigger magnets have larger magnetic moments (hence, larger $\|\vec{m}_i\|$ and $\|\vec{m}_j\|$ in Eqs. (1) and (2)), as the magnetic moment is directly proportional to magnet volume. In general, the trend shows that the larger the magnets become, the higher the output torque of the motor becomes without showing much tendency to converge. We therefore chose a set of 3 mm cubic magnets in this study, rather than a set of 4 mm magnets for a motor, to reduce the size of the overall motor.

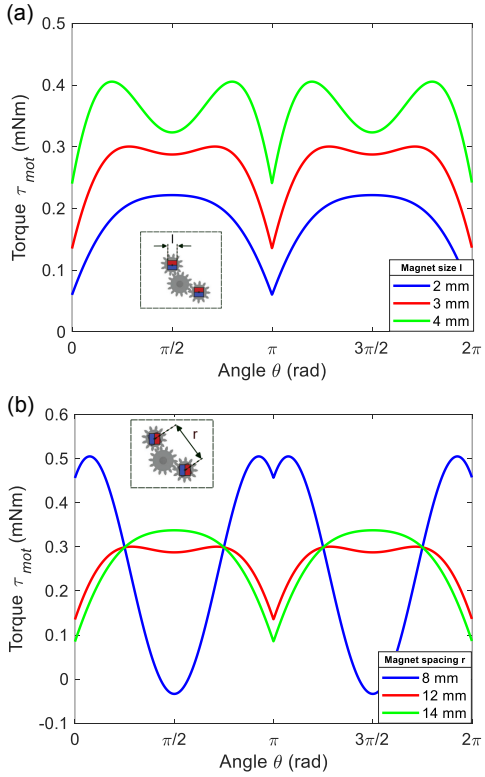

Fig. 3. The theoretical model of output motor torque (τ_{mot}) while changing (a) the magnets' sizes (constant magnet spacing $\|\vec{r}_{ij}\| = 12$ mm), and (b) the inter-magnet distance or magnet spacing (constant magnet size $3 \times 3 \times 3\,\text{mm}^3$).

The next step is to choose the optimum distance between the magnets or the magnet spacing, r, in the motor. We change the magnitude of $\vec{r}_{ij}$ in Eq. (1), while keeping the magnet size constant, $3 \times 3 \times 3\,\text{mm}^3$. In general, the motor torque increases as the distance between the magnets decreases (Fig. 3 (b), assuming that B_{ext} is 7 mT which is our operation magnetic flux density in experiments). At the other extreme, the internal torque becomes too large if the magnets are too near to each other. In that case, the external torque generated from the coils will not be sufficient to rotate and align the magnets (note that the motor torque alternates between positive and negative when the magnets are too close at 8 mm spacing, Fig. 3 (b)). Thus, the motor will fail to complete a full cycle. We chose a spacing of 12 mm at $B = 7$ mT to find the optimum balance between the internal and external torques.

2) Step-out frequency: The angular velocity of the motor, ω, is proportional to the actuation frequency of the external field (f_a), up to the step-out frequency of the motor (f_{so}).

When the actuation frequency exceeds the motor step-out frequency, the magnets cannot keep up with the fast field reversals, due to their inherent inertia. The relationship between the angular velocity of the motor and the actuation frequency of the external field can be expressed as [28], [29]:

$$\omega = \begin{cases} 2\pi f_a, & \text{if } f_a < f_{so} \\ 2\pi(f_a - \sqrt{f_a^2 - f_{so}^2}), & \text{if } f_a > f_{so} \end{cases}. \quad (4)$$

C. Zero net torque dual-motor system

Unlike other magnetically-actuated motors previously reported in the literature, such as [2], the motors developed in this study are actuated with a reversible bi-axial magnetic field rather than a rotating magnetic field. We utilize this feature to develop a dual-motor system that experiences a net-zero torque to prevent any undesired rotational motion of the overall system. Fig. 4 shows a schematic of the developed system, which consists of two motors arranged symmetrically about the center of rotation of the system (for a total of four permanent magnets). The two motors generate torques with the same magnitude but in opposite directions.

Each motor operates analogously to the configuration shown in Fig. 1. The electromagnetic coils generate an external magnetic field and the magnetic moments of the four magnets align along the field direction (Fig. 4 (a), state $F^D(1)$), at that point the external torque drops to zero. After that, the applied magnetic field reverses direction. Each motor continues to rotate as the magnetic moments of the embedded magnets align along a common axis due to their mutual attraction (Fig. 4 (b), state $F^D(2)$). This interplay between the internal and external torques continues as the magnets align to the newly established field direction (Fig. 4 (c), state $F^D(3)$) until both motors finish a full cycle after the field reverses again (Fig. 4 (d), state $F^D(4)$). The dual-motor system can operate in reverse by applying a reversible uni-axial magnetic field along the perpendicular direction (Fig. 4 (e) to (h), states $B^D(1)$ to $B^D(4)$).

III. Methods

A. Fabrication of the motor

An SLA 3D printer (Elegoo Saturn 3 Ultra 12K, XY Resolution of 19×24 μm) and Water washable photopolymer resin was used to fabricate the gears and the motor body. A 3 mm cubic neodymium (NdFeB, N42) magnet (Supermagnete) was glued to the center of each magnet gear. The magnet gears have 12 teeth and 0.5 mm module. These gears mesh with a central output gear connected to the output shaft, which transmits the torque generated by the motor. The output gear at the center of the motor has 14 teeth giving a gear ratio of $1:1.17$. The dual-motor system is attached to a 3D printed support platform (platform length is 52 mm, width is 19 mm, height is 32 mm).

We demonstrate the performance of the dual-motor system by attaching a gripper arm to each motor (see Section IV-B, Fig. 8). The gripper arms are also made of Water washable photopolymer resin and coupled to the output shaft at the center of the output gear of each motor (gripper arm length is 25 mm). Two sets of reduction gears placed between the gripper and the motors ensure the smooth operation of the gripper mechanism (the reduction gear module is 0.5 mm). The input reduction gear has 11 teeth while the output reduction gear has 21 teeth. Thus, the gear ratio of the reduction gears is $1:1.9$.

To demonstrate that the dual-motor system and the attached gripper experience zero net torque during operation, the entire system is fit inside a custom-built floater. This floater floats to the water surface at the center of a tank positioned between four electromagnetic coils (see Fig. 8).

B. Motor actuation by electromagnetic coils

We generate a reversible uni-axial magnetic field using two parallel electromagnetic coils with a square cross-section (side length is 200 mm, the distance between coils is 225 mm, and the input current is 35 A). In some experiments, we need to reverse the rotation of the motor from clockwise to counter-clockwise and vice-versa. In these tests, we use four coils oriented perpendicular to each other (Fig. 5). We use 4 coils, rather than the required 2, to improve the uniformity of the field in the workspace. Magnetic flux densities of up to 7 mT were applied from the coils at different frequencies below the step-out frequency. The flux densities used in this study are well below the static magnetic flux density of $0.046 - 8$ T of MRI machines [30], this shows that these magnetic fields can safely be used in a medical setting. All coils were controlled using Sabertooth 2×32 motor drivers.

IV. Results

A. A single motor

We investigated the evolution of the output torque of the developed magnetic motor while varying the strength of the external magnetic field. The output shaft of the motor was attached to a string that passed through a pulley and ended with an object to lift. The torque was calculated by determining the maximum weight that the motor could lift in response to the applied magnetic field. The motor could lift the object if the required torque was less than the minimum motor torque. On the other hand, the motor stalled when the required torque was higher than τ_{mot}. We repeated this experiment at different magnetic flux densities (Fig. 6).

As the experimental data shows, the motor was unable to deliver any output torque when the magnetic flux density was lower than 2.8 mT. At that low magnetic flux density, the produced external magnetic torque was not sufficient to overcome the internal magnetic torque. Beyond 2.8 mT, the motor could start lifting the suspended object. The trend shows that as the magnetic flux density increased, τ_{mot} increased. Eventually, τ_{mot} saturated at $\tau_{mot} = 0.07$ mNm, above which it remained constant despite the increase of the magnetic flux. At that point, the generated external magnetic torque became too large and dominated the internal magnetic torque.

The line shown in black in Fig. 6 shows the theoretical plot of τ_{mot} derived from Eqs. (1), (2) and (3). The model shows

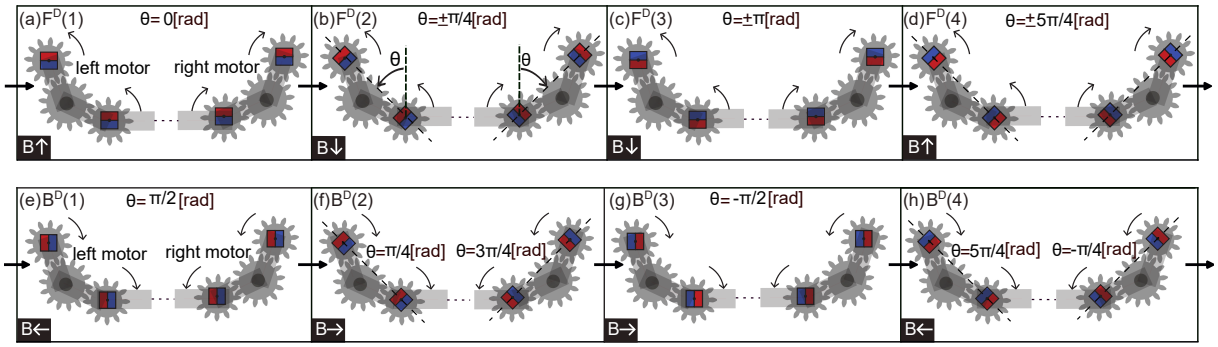

Fig. 4. Schematic diagram showing the operation mechanism of the dual-motor system. In states $F^D(1)$ to $F^D(4)$, the two motors undergo forward rotation. In states $B^D(1)$ to $B^D(4)$, the motors rotate in reverse. The figure also shows the direction of the applied external magnetic flux (B_{ext}) depicted in the same way as in Fig. 1.

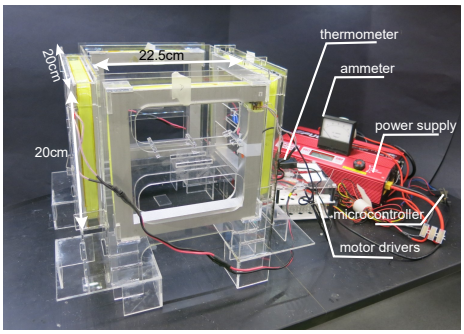

Fig. 5. The coil system used for motor actuation. This system consists of four perpendicular electromagnetic coils that generate bi-axial magnetic fields along two perpendicular directions. The motor is placed at the center of the coil system.

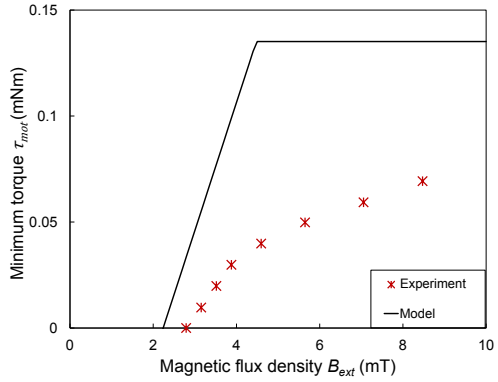

Fig. 6. Minimum output torque delivered by the motor shaft at different magnetic flux densities. The red markers show experimental measurements of the torque, while the black line shows the model results, Eqs 1, 2 and 3.

a similar trend to the experimental results, whereby τ_{mot} increased as B_{ext} increased and then saturated. There were some discrepancies between the model and the experimental results, as the model overestimated the motor torque. The friction between the different components of the motor reduces the output motor torque, which might explain this discrepancy.

We then calculated the angular velocity of the motor by analyzing videos recorded during its revolution and estimating the time the gears take to complete a full cycle. Fig. 7 shows the relationship between the actuation frequency and the angular velocity of a single motor without any attached load and with a 1 g load. The angular velocity

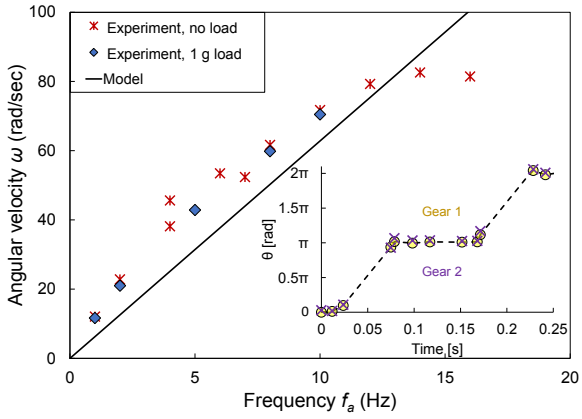

Fig. 7. Angular velocity of the motor as a function of the actuation frequency. This figure compares experimental data (the red marker shows the data while the motor is not loaded, and the blue marker shows the data while the motor is loaded with 1g of weight) and model results (a continuous black line shows how our model-Eq. 4- predicts angular velocity while the motor is not loaded with any weight). The inset shows the motor orientation θ as a function of time for gear 1 (yellow) and 2 (violet), frequency=4 Hz

increases proportionally with the actuation frequency before it saturates at $\omega = 80$ rad/sec, beyond which it remains constant with a further increase of frequency. Experimental data agrees well with the developed model (Eq. (4)) at low frequencies. The angular velocity of the motor without a load is slightly higher than the velocity measurements with an attached load. The added load increases the moment of inertia of the overall system and decreases the net torque and angular velocity of the motor, as a direct consequence of Newton's second law of motion. At high frequencies beyond 10 Hz, the motor sometimes experiences unstable negative revolution due to the rapid field reversals. This trend is expected to become more pronounced as the load increases, but load torque is not considered to be so significant a factor since it can be handled to a good extent by increasing the gear ratio of the reduction gear of the motor.

B. Dual motor system with rotation-free gripper

The developed magnetic motor can cancel out the torque by placing another mirrored motor within the structure. This

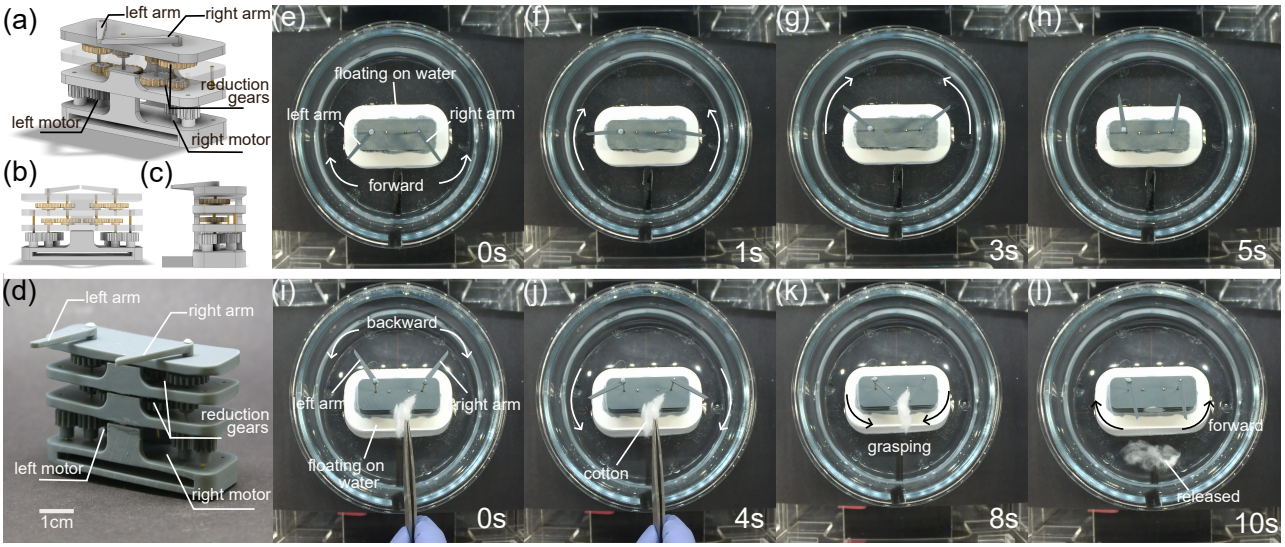

Fig. 8. Dual motor system with the free-floating gripper. CAD design in (a) angled, (b) front and (c) side view. (d) Photo of the dual-motor system with the attached gripper arms. The gripper arms rotate forward (e to h) and background (i to k) in response to an external magnetic flux B_{ext} while floating on the surface of the water. The gripper grasps and holds onto a piece of cotton (j) and (k) before releasing it upon reversing its rotation one final time (l). The dual-motor system is not supported and experiences zero net torque. See also supplementary video.

arrangement allows the dual-motor system to generate an output torque in a magnetic field without rotating the overall device, even in a situation where the device is not fixed to the environment. To demonstrate this feature, we built a mobile gripper (appearing in Fig. 8 (a-d)) with two magnetic motors arranged symmetrically as depicted in Fig. 4, and demonstrated that it can be driven in an environment where rotation in the yaw direction is allowed, i.e. on water. In the gripper, the output shafts from each motor are coupled to the respective gripper arms. We define that the gripper makes a 'forward' rotation if the left motor and the attached gripper arm rotate clockwise.

We placed the dual-motor system on the water surface in a tank placed at the center of the coil setup to ensure a 'quasi' uniform magnetic field. We then applied a reversible magnetic field along the x-direction (following the local coordinate system shown in Fig. 1 (a)) at a relatively low frequency of 0.33 Hz, and briefly turned off the coils after the magnets align to the applied field direction, for easier observation and better visualization of motor performance. Note that the gripper and the dual-motor system were not supported or fixed at any point in time, but were freely floating on the water surface throughout the test. It can be seen that the two motors responded to the external magnetic field and thus the gripper arms rotate 'forward' (Fig. 8 (e) to (h)). We then applied a magnetic field along the perpendicular direction, which prompted the two motors, and hence the gripper arms, to reverse their rotation (Fig. 8 (i)). During this backward rotation, we held a piece of cotton near the gripper until the arms grasped it (Fig. 8 (j)). We then released the object, but the gripper arms continued to hold onto and support it in place (Fig. 8 (k)). Finally, we applied a field along the x-direction, and the arms reversed their rotation once more to the 'forward' direction, thus releasing the object (Fig. 8 (l)). Throughout the entire cycle, the dual-motor system along with the gripper did not experience a net torque or any undesired rotation, even in the absence of a reactive frictional force, showcasing the ability of the motor. In contrast, the gripper rotates when we remove one of the two motors, as shown in the supplementary video. Such a gripping mechanism could potentially be implemented into a robot that samples or moves objects in a confined space.

V. Conclusion

In this study, we develop a wirelessly actuated magnetic motor composed of two permanent magnets embedded in gears. The motor rotates in response to a reversible bi-axial magnetic field. The rotation of the motor can be reversed simply by applying a field in the perpendicular direction. The rotation of the gears results from the interplay between the internal torque due to the mutual interaction of the magnets and the external torque generated due to the external magnetic field. The model shows that a minimum torque is guaranteed throughout the duration of one motor revolution, albeit the torque increases and decreases within a single cycle. We use the model to study the effect of different design variables on the output torque to optimize motor performance. The experiments show that the motor does not behave unwillingly (e.g. rotating in the reverse direction) within certain operation frequencies, even when a load exceeding the minimum torque of the motor is applied. This study also highlights the potential of the magnetically actuated motor in practical applications. The experiment showcasing the actuation of the gripper demonstrates that the dual-motor system experiences net zero motor torque. The unsupported gripper can open and close its arms, thus grasping and releasing an object without experiencing any undesired rotations throughout its operation.

Acknowledgment

We thank Xiao Chen and Junyi Han for their assistance in conducting the experiments and reviewing the paper.

REFERENCES

[1] B. Yigit, Y. Alapan, and M. Sitti, "Programmable collective behavior in dynamically self-assembled mobile microrobotic swarms," *Advanced Science*, vol. 6, no. 6, p. 1801837, 2019.

[2] C. Hong, Z. Ren, C. Wang, M. Li, Y. Wu, D. Tang, W. Hu, and M. Sitti, "Magnetically actuated gearbox for the wireless control of millimeter-scale robots," *Science robotics*, vol. 7, no. 69, p. eabo4401, 2022.

[3] W. Lee, J. Nam, J. Kim, E. Jung, and G. Jang, "Effective locomotion and precise unclogging motion of an untethered flexible-legged magnetic robot for vascular diseases," *IEEE Transactions on industrial electronics*, vol. 65, no. 2, pp. 1388–1397, 2017.

[4] S. Terryn, J. Brancart, D. Lefeber, G. Van Assche, and B. Vanderborght, "Self-healing soft pneumatic robots," *Science Robotics*, vol. 2, no. 9, p. eaan4268, 2017.

[5] M. Sun, S. Yang, J. Jiang, S. Jiang, M. Sitti, and L. Zhang, "Bioinspired self-assembled colloidal collectives drifting in three dimensions underwater," *Science Advances*, vol. 9, no. 45, p. eadj4201, 2023.

[6] M. N. I. Shiblee, K. Ahmed, M. Kawakami, and H. Furukawa, "4d printing of shape-memory hydrogels for soft-robotic functions," *Advanced Materials Technologies*, vol. 4, no. (8), p. 1900071, 2019.

[7] S. Miyashita, S. Guitron, S. Li, and D. Rus, "Robotic metamorphosis by origami exoskeletons," *Science Robotics*, vol. 2, no. 10, p. eaao4369, 2017.

[8] H. Park, S. Park, E. Yoon, B. Kim, J. Park, and S. Park, "Paddling based microrobot for capsule endoscopes," in *Proceedings 2007 IEEE International Conference on Robotics and Automation*, 2007, pp. 3377–3382.

[9] A. Hajiaghajani, D. Kim, A. Abdolali, and S. Ahn, "Patterned magnetic fields for remote steering and wireless powering to a swimming microrobot," *IEEE/ASME Transactions on Mechatronics*, vol. 25, no. 1, pp. 207–216, 2019.

[10] Y. Kim, J. E. Park, J. J. Wie, S. G. Yang, D. H. Lee, and Y.-J. Jin, "Effects of helix geometry on magnetic guiding of helical polymer composites on a gastric cancer model: A feasibility study," *Materials*, vol. 13, no. 4, p. 1014, 2020.

[11] Y. Ju, R. Hu, Y. Xie, J. Yao, X. Li, Y. Lv, X. Han, Q. Cao, and L. Li, "Reconfigurable magnetic soft robots with multimodal locomotion," *Nano Energy*, vol. 87, p. 106169, 2021.

[12] X. Hu, I. C. Yasa, Z. Ren, S. R. Goudu, H. Ceylan, W. Hu, and M. Sitti, "Magnetic soft micromachines made of linked microactuator networks," *Science advances*, vol. 7, no. 23, p. eabe8436, 2021.

[13] D. Son, M. C. Ugurlu, and M. Sitti, "Permanent magnet array–driven navigation of wireless millirobots inside soft tissues," *Science Advances*, vol. 7, no. 43, p. eabi8932, 2021.

[14] J. Han, D. Rus, and S. Miyashita, "Roblets: Robotic tablets that self-assemble and self-fold into a robot," in *2023 IEEE/RSJ International Conference on Intelligent Robots and Systems (IROS)*, 2023, pp. 4709–4714.

[15] K. Ishiyama, M. Sendoh, A. Yamazaki, and K. Arai, "Swimming micro-machine driven by magnetic torque," *Sensors and Actuators A: Physical*, vol. 91, no. 1-2, pp. 141–144, 2001.

[16] J. J. Abbott, Z. Nagy, F. Beyeler, and B. J. Nelson, "Robotics in the small, part i: microbotics," *IEEE Robotics & Automation Magazine*, vol. 14, no. 2, pp. 92–103, 2007.

[17] M. Nokata, S. Kitamura, T. Nakagi, T. Inubushi, and S. Morikawa, "Capsule type medical robot with magnetic drive in abdominal cavity," in *2008 2nd IEEE RAS & EMBS International Conference on Biomedical Robotics and Biomechatronics*, 2008, pp. 348–353.

[18] L. Zhang, J. J. Abbott, L. Dong, B. E. Kratochvil, D. Bell, and B. J. Nelson, "Artificial bacterial flagella: Fabrication and magnetic control," *Applied Physics Letters*, vol. 94, no. 6, 2009.

[19] B. J. Nelson, I. K. Kaliakatsos, and J. J. Abbott, "Microrobots for minimally invasive medicine," *Annual review of biomedical engineering*, vol. 12, pp. 55–85, 2010.

[20] M. Sitti, H. Ceylan, W. Hu, J. Giltinan, M. Turan, S. Yim, and E. Diller, "Biomedical applications of untethered mobile milli/microrobots," *Proceedings of the IEEE*, vol. 103, no. 2, pp. 205–224, 2015.

[21] S. Martel, "Beyond imaging: Macro-and microscale medical robots actuated by clinical mri scanners," *Science Robotics*, vol. 2, no. 3, p. eaam8119, 2017.

[22] A. Hafez, Q. Liu, and J. C. Santamarina, "Magneto-rheological fluids: tele-manipulation of ferromagnetic particles with external magnetic field for flow control and zonal isolation," *Geoenergy Science and Engineering*, vol. 228, p. 212029, 2023.

[23] A. Sinha, R. Ganguly, A. K. De, and I. K. Puri, "Single magnetic particle dynamics in a microchannel," *Physics of Fluids*, vol. 19, no. 11, 2007.

[24] E. Diller, J. Giltinan, G. Z. Lum, Z. Ye, and M. Sitti, "Six-degree-of-freedom magnetic actuation for wireless microrobotics," *The International Journal of Robotics Research*, vol. 35, no. 1-3, pp. 114–128, 2016.

[25] C. Duffield and S. Miyashita, "Magnetic force driven wireless motor," in *Towards Autonomous Robotic Systems: 21st Annual Conference (TAROS)*. Springer, 2020, pp. 409–412.

[26] C. Duffield, A. F. Smith, D. Rus, D. Damian, and S. Miyashita, "Wirelessly magnetically actuated motor for tissue regeneration robotic implant," in *IEEE/RSJ International Conference on Intelligent Robots and Systems (IROS)*, 2022, pp. 465–471.

[27] P. B. Landecker, D. D. Villani, K. W. Yung *et al.*, "An analytic solution for the torque between two magnetic dipoles," *Physical Separation in Science and Engineering*, vol. 10, pp. 29–33, 1999.

[28] T. A. Howell, B. Osting, and J. J. Abbott, "Sorting rotating micromachines by variations in their magnetic properties," *Phys. Rev. Appl.*, vol. 9, p. 054021, May 2018. [Online]. Available: https://link.aps.org/doi/10.1103/PhysRevApplied.9.054021

[29] K. I. Morozov and A. M. Leshansky, "The chiral magnetic nanomotors," *Nanoscale*, vol. 6, pp. 1580–1588, 2014. [Online]. Available: http://dx.doi.org/10.1039/C3NR04853E

[30] S. A. Alghamdi, S. A. Alshamrani, O. I. Alomair, Y. I. Alashban, A. H. Abujamea, E. H. Mattar, M. Almalki, and M. Alkhorayef, "Safety survey on lone working magnetic resonance imaging technologists in saudi arabia," in *Healthcare*, vol. 11, no. 5. MDPI, 2023, p. 721.